Oxygen-reducing bidirectional microbial electrodes designed in real domestic wastewater

Morgane Hoareau [a], Benjamin Erable [a], Olivier Chapleur [b], Cédric Midoux [b], Chrystelle Bureau [b], Anne Goubet [b], Alain Bergel [a,*]

[a] Laboratoire de Génie Chimique, Université de Toulouse, CNRS, INP, UPS, Toulouse, France
[b] Université Paris-Saclay, INRAE, PRocédés biOtechnologiques au Service de l'Environnement, 92761 Antony, France

HIGHLIGHTS

- In anode operation, current density up to 6.4 A.m^{-2} were produced in real wastewater.
- Bioanodes formed in open-to-air reactor gave higher O$_2$-reduction current when aerated.
- *Gammaproteobacteria*, *Bacteroidia* and *Clostridia* were the three dominant classes.
- Clear distinction between the planktonic and sessile microbial populations.
- Biofilm microbial population mixed both aerobic and anaerobic electroactive species.

ARTICLE INFO

ABSTRACT

Microbial electrodes were designed in domestic wastewaters to catalyse the oxidation of organic matter (anode) and the reduction of oxygen (cathode) alternately. The successive aeration phases (cathode) enhanced the anodic efficiency, resulting in current densities of up to 6.4 Am^{-2} without the addition of any substrate. Using nitrogen during the anodic phases affected the microbial populations and the electrodes showed a lower ability to subsequently turn to O$_2$ reduction than the microbial anodes formed in open-to-air conditions did. No strong difference was observed between internal and external biofilm, both of which showed a very large variety of taxa in terms of abundance as well as variance. They comprised a mix of aerobic and anaerobic species, many of which have already been identified separately in bioelectrochemical systems. Such a large diversity, which had not been observed in aerobic bidirectional bioelectrodes so far, can explain the efficiency and robustness observed here.

1. Introduction

A platinum electrode polarized at a constant potential (in the range where water electrolysis does not occur) can be an anode when supplied with hydrogen or a cathode when supplied with oxygen. Such bidirectional electron transfer is usual in the domain of abiotic electrochemistry. Microbial electrodes can also achieve bidirectional electron transfer, but generally in fully anaerobic conditions, i.e. by using electron acceptors such as nitrate, sulfate or carbon dioxide in the cathodic mode (Kalathil and Pant, 2016; Xie et al., 2020) rather than oxygen. Actually, it was initially thought that oxygen was drastically detrimental to exoelectrogen biofilms because it can kill strictly anaerobic exoelectrogen bacteria and, in contrast, it can promote the development of aerobic non-electroactive bacteria. This vision has gradually changed, as some microbial anodes have been observed to tolerate oxic environments while still maintaining high efficiency (Erable and Bergel, 2009) and even to benefit from micro-aeration (Yong et al., 2017; Yang et al., 2018).

A few studies have now demonstrated that microbial electrodes can achieve bidirectional electron transfer with oxygen as the electron acceptor. The aerobic bidirectional electrodes (ABMEs) catalyse the oxidation of organic matter in anoxic conditions and the reduction of oxygen in aerobic conditions (Jiang and Zeng, 2019). ABMEs have already shown great promise for pH stabilisation in microbial fuel cells (MFC). In an MFC, oxidation of the organic matter acidifies the anode, while reduction of oxygen alkalinises the cathode.

Both pH drifts result in considerable decrease of the MFC performance (Oliot et al., 2016). Designing an MFC with an ABME in each compartment allows the anode and cathode modes be alternated on each electrode (Cheng et al., 2010; Li et al., 2014). This strategy has proved successful in stabilising the pH value of MFCs around a neutral value for more than 140 days (Strik et al., 2010). A recent study has shown that ABMEs implemented on rotating disks partially exposed to air have great potential for wastewater treatment (Chen et al., 2019a). ABMEs would also inevitably occur in microbial snorkels (Hoareau et al., 2019).

A microbial snorkel can be considered as a short-circuited MFC and can be as simple as a single electrode with its lower part (anode) in the anoxic bottom of a wastewater treatment tank and the upper part (cathode) in the aerated zone of the reactor (Erable et al., 2011). The principle of the microbial snorkel has been successfully implemented in the form of conductive granular beds in constructed wetlands (Aguirre-Sierra et al., 2016; Domínguez-Garay and Esteve-Núñez, 2018; Quejigo et al., 2019). In a snorkel, the frontier between the oxic and anoxic zones is often not well-defined and can move to a great extent because of the wastewater loading sequence, the application of stirring or not, wind and rain affecting the outdoor wetlands, etc. In consequence, although it has not been pointed out in the literature so far, ABMEs must inevitably be created in the fuzzy anoxic/oxic zone of microbial snorkels.

In spite of such a variety of applications, the number of studies devoted to ABMEs remains limited. Most of the studies have used synthetic media (Freguia et al., 2008; Strik et al., 2010; Cheng et al., 2010; Li et al., 2014; Sun et al., 2015; Yu et al., 2015). Only two have used a natural medium, leachate from garden compost (Blanchet et al., 2014) or wastewater (Chen et al., 2019a). All have added an artificial substrate: acetate (Freguia et al., 2008; Cheng et al., 2010; Strik et al., 2010; Blanchet et al., 2014; Yu et al., 2015) or glucose (Li et al., 2014; Sun et al., 2015), as the carbon source. Only a few studies have explored the microbial populations related to ABMEs.

The purpose of the present study was to assess the possibility of designing ABMEs in raw domestic wastewater and to gain information for possible future application of ABMEs in wastewater treatment. The study intended to determine the effect of the anoxic/oxic conditions on the electrode performance and biofilm composition.

The experiments were carried out in electroanalytical conditions in order to fix as many parameters as possible (Rimboud et al., 2014) apart from the anoxic/oxic conditions. In particular, the potential of the electrodes was controlled at a constant value by using 3-electrode set-ups. The potential of -0.1 V/SCE was chosen in these cases because this value has provided both efficient microbial anodes (Roubaud et al., 2019) and O_2-reducing microbial cathodes (Milner et al., 2016) when activated sludge was used as the inoculum. Electrodes had a small surface area (2×4 cm^2) in comparison to the volume of solution (more than 2.5 L) in order to stabilise the chemical composition of the solution over long periods. The cathode phases were brought about simply by setting forced aeration. The microbial populations were analysed in relation to biofilm age, biomass location – on the outer surface or inside the carbon felt electrodes – and the level of anoxia maintained during the anode phases.

2. Materials and methods

2.1. Media and set-up

The electrochemical reactors were Schott flasks containing 500 mL of domestic wastewater (WW) collected from the aerobic tank of a wastewater treatment plant (Castanet-Tolosan, near Toulouse, France). They were inoculated with 5% (v/v) activated sludge from the same plant. The concentrations of total suspended solids (TSS) and volatile suspended solids (VSS) of the sludge were 10 ± 1 and 8.7 ± 0.1 g.L^{-1}, respectively. All the reactors were initially filled with fresh mix of WW and 5% sludge. This mix had initial values of soluble and total COD of 230 and 1230 mg O$_2$.L^{-1}, respectively, and the initial pH was 8.3. Each

reactor was part of a closed hydraulic loop including a peristaltic pump (Masterflex®, Cole-Parmer, USA) and a 2 L storage tank. The storage tanks always contained hydrolysed WW. Hydrolysis consisted of keeping the WW in a closed tank under anaerobic conditions at room temperature for one week. This step promoted hydrolysis of the particulate COD and thus maximized the soluble COD. Depending on the different times of WW collection, the COD of hydrolysed WW was in the range of 250–350 mg O$_2$.L^{-1} (against 150–250 mg O$_2$.L^{-1} for WW before hydrolysis).

Each reactor was equipped with a 3-electrode set-up. The working electrodes were carbon felt sheets (RVG 4000, Mersen, France) (Blanchet et al., 2016) of 2×4 cm^2 surface area and 0.5 cm thickness. They were electrically connected with titanium rods (1 mm in diameter) with the free part insulated by heat-shrinkable sleeves. The working electrodes were placed at the free surface of the solution so as to have easy access to oxygen during cathodic phases. The 16 cm^2 counter electrodes were made of carbon cloth (Paxitech, France) and were connected to the electrical circuit with a platinum wire. A multi-channel potentiostat (MPG, EClab software, Bio-Logic SA) was used to control the potential of each working electrode vs. a saturated calomel reference electrode (SCE, Sentek, Australia, 0.24 V/SHE). All potentials were expressed vs. SCE. Biofilms were formed and operated under a constant applied potential of -0.1 V vs. SCE and at room temperature (20 ± 2 °C). The current density (A.m^{-2}) was related to the projected surface area of the working electrode, 8 cm^2.

2.2. Biofilm formation and operation (Fig. 1)

Eight reactors were run in parallel. Four were run under continuous bubbling of N$_2$ while the other four had no bubbling and remained open to the air. The first 28 days were dedicated to the formation of microbial anodes and there was no switch in cathodic conditions during this period. This anode formation phase started in batch mode (no solution circulation). An increase of the current indicated the formation of an electroactive biofilm on the working electrode. When the current stopped rising, around day 8, the closed hydraulic loop was put into circulation mode at a flow rate of 1.5 mL.min^{-1}. When the current dropped, the COD in the loops was no longer sufficient and the storage tanks were changed to provide the reactors with hydrolysed WW. The storage tanks were always changed at the same time for the eight loops, at days 9, 17 and 24.

After day 28, anodic and cathodic phases were alternated. Cathodic phases were started when the substrate contained in the recirculating loop had been consumed, which was detected by the current dropping to near zero. Recirculation was stopped, all eight reactors were opened and air bubbling was set up. Four cathodic phases were completed on days 28, 35, 38 and 44, each lasting for approximately 24 h. At the end of the cathodic phases, the storage tanks were changed to provide the reactors with COD again (days 30, 36, 39, 46) and the anodic conditions were restored. The storage tanks were also changed at days 42 and 49. Two reactors (one under nitrogen and one not) were stopped at day 28, and two others at day 38, in order to analyse the evolution of the microbial populations.

Electrodes were characterised by cyclic voltammetry (CV) from -0.6 to 0.4 V/SCE at 1 mV.s^{-1}. CVs were performed at the beginning and the end of the experiments and at important times (change of conditions, aeration, etc.). For each CV, three cycles were recorded. The first cycle was sometimes slightly different from the next two cycles, which were usually identical. The second cycles are represented in this article.

Throughout the experiment, Chemical Oxygen Demand (COD) was measured using Hach Lange LCK 514 microkits for a concentration ranging from 100 to 2,000 mg of O$_2$.L^{-1} and LCK 314 for concentrations ranging from 15 to 150 mg of O$_2$.L^{-1}. Soluble COD was measured after filtering the samples with a syringe filter having a pore diameter of 0.22 μm.

Oxygen concentrations were measured with an optical dissolved

oxygen meter Multi 3410 (WTW GmbH, Germany) in the middle of the reactors, i.e. around 10 cm below the free surface of the solution.

2.3. Molecular biology methods

After the shutdown of the reactors, a 3 cm^2 piece of the felt electrode and 10 mL of culture medium were collected for molecular biology analyses. The external biofilm was recovered by scraping the surface of the electrode with a scalpel. After removal of the external biofilm, the internal biofilm was collected by placing the felt pieces in an ultrasonic bath for 15 min. All samples were then centrifuged for 15 min at 4600 g and 6 °C. DNA extraction was performed on the pellet of each sample using a DNeasy PowerBiofilm (Qiagen) kit, according to the manufacturer's recommendations.

2.3.1. 16S sequencing

16S rRNA gene high-throughput DNA sequencing was performed at the NGS facility of the PROSE Research Unit, INRAE (Antony, France) using Ion Torrent™ (Life Technologies, USA) technology and methods. Archaeal and bacterial hyper variable region V4-V5 of the 16S rRNA gene was amplified and then sequenced according to the protocol described by Poirier et al. (2016) or Madigou et al. (2019) with some modifications.

The V4–V5 region was amplified according to the Platinum SuperFi DNA Polymerase 3-step protocol (Invitrogen). PCR products were purified using Solid Phase Reversible Immobilization (SPRI) magnetic beads (Mag-Bind TotalPure NGS magnetic beads, Omega Bio-Tek) according to the manufacturer's instructions. Purified amplicons were quantified using D1000 ScreenTape and 2200 TapeStation (Agilent Technologies). Then all amplicons were pooled in equimolar ratios.

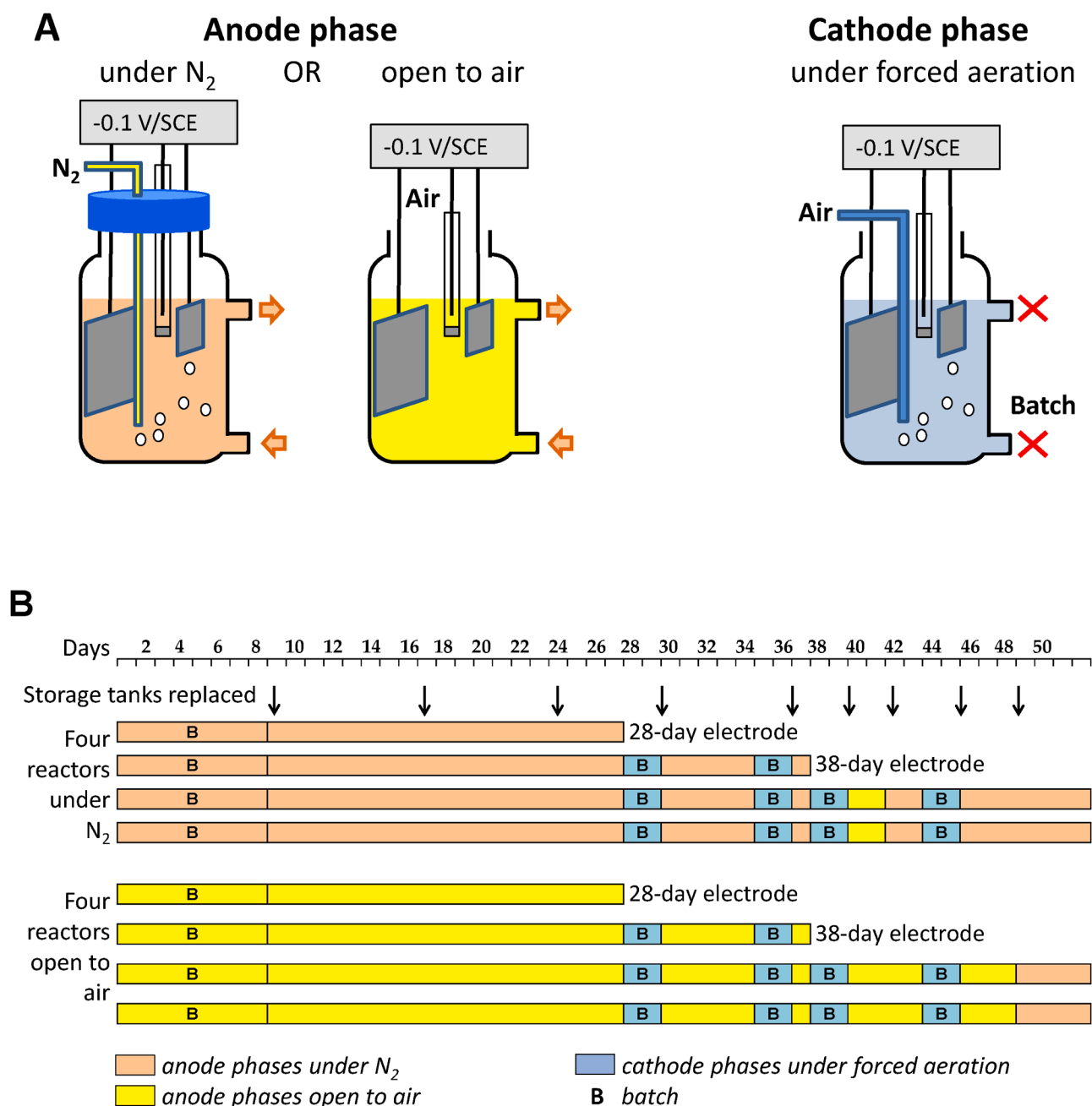To prepare template-positive Ion Sphere Particles (ISPs), the library

Fig. 1. Scheme of the experimental set-up and timetable of the protocol.

was set up on the Ion OneTouch 2 Instrument (Life Technologies) using the Ion PGM Hi-Q View OT2 Kit (Life Technologies) and following the manufacturer's instructions.

Sequencing was performed on an Ion Torrent Personal Genome Machine using Ion 316 Chip V2 (Life Technologies) and Ion PGM Hi-Q View Sequencing Kit (Life Technologies) according to the manufacturers' instructions. Sequencing data was processed by the Torrent Suite Software. The software filtered out low quality and polyclonal sequence reads, and filtered data was exported as a FastQ file.

2.3.2. Data treatments

An OTU (operational taxonomic unit) count matrix was designed using a FROGS (Find Rapidly OTU with Galaxy Solution) (Escudié et al., 2018) pipeline, including DNA quality controls, metabarcoding sequence analyses, and OTU affiliation using blastn with 16S_silva132 database. Low abundance OTUs were filtered out and OTUs present at
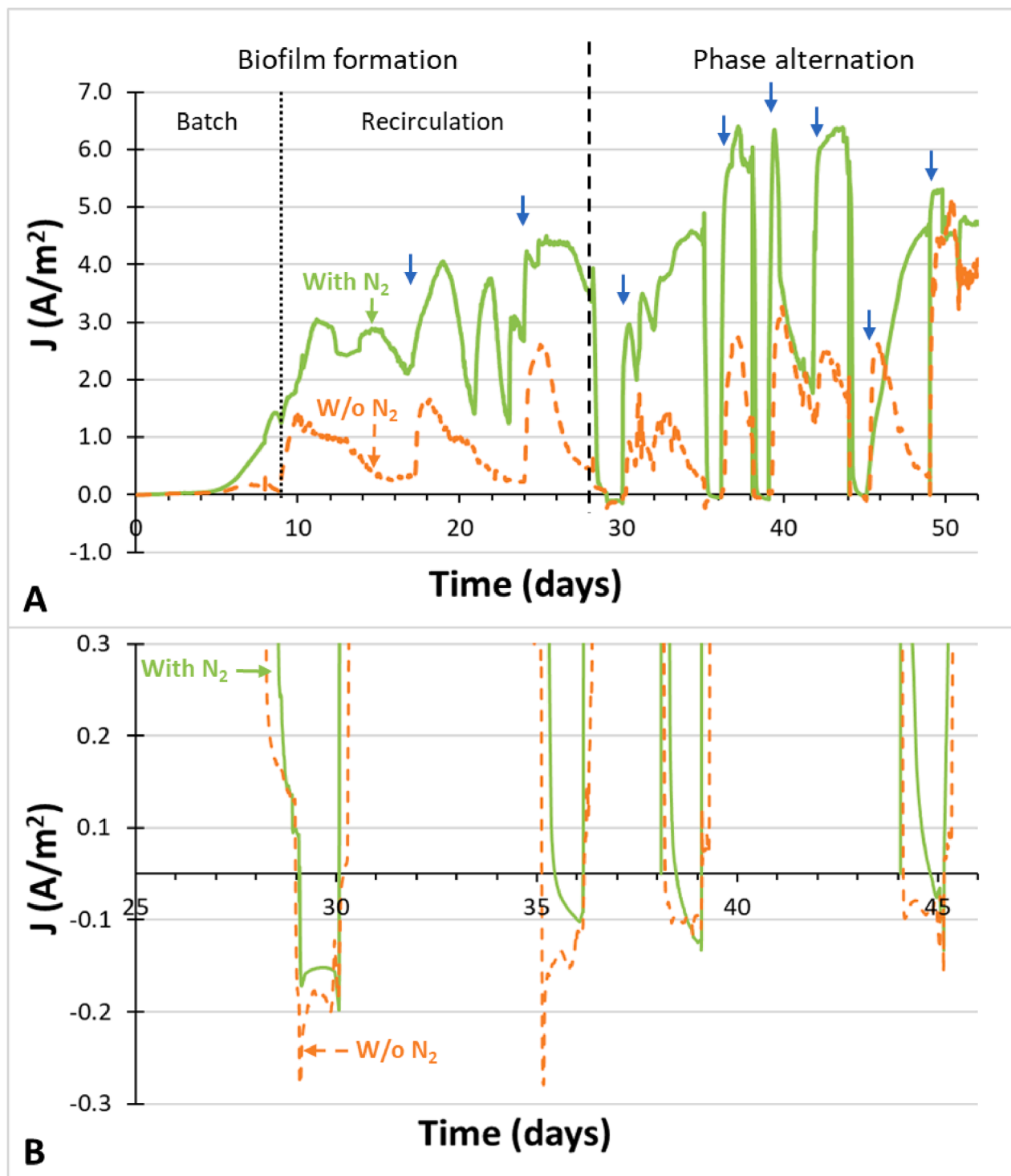
Fig. 2. Current density versus time under constant polarization at -0.1 V/SCE. Average values of the electrode operated with N_2 (green) or without N_2 supply (orange). (A) Entire experiment (days 0 to 52) and (B) focus on the cathodic phases. After 9 days in batch mode, the recirculation was started (dotted line). After day 28, cathodic and anodic phases were alternated (dashed line). Arrows indicate the storage tank changes.

above 0.5% in at least one sample were kept. The OTU abundances were examined using R CRAN software (version 3.6), phyloseq and mixOmics R packages. Principal Component Analysis (PCA) was performed to highlight the relationship between samples from the different conditions after OTU abundances in the samples had been transformed with centred log ratio (CLR) (Rohart et al., 2017).

3. Results and discussion

3.1. Electrochemical results

Eight reactors were operated under constant applied potential at -0.1 V/SCE. Four reactors were under nitrogen bubbling and four with no nitrogen supply remained open to the air (Fig. 1). Fig. 2 gives the average curves for each of the two conditions. The first 28 days (Fig. 2.A) were used to form microbial anodes. They gave results similar to those already reported in identical conditions (Roubaud et al., 2019). During this biofilm formation phase, the values of current in the reactors with N_2 bubbling reached 4.1 ± 0.8 A.m^{-2}, which was the level of the highest values reported for microbial anodes designed in raw WW without acetate addition. It was twice the steady state current density of 2.0 A.m^{-2} obtained in similar domestic wastewater with carbon felt electrodes (Roubaud et al., 2019). To the best of our knowledge, the highest current density reported in similar conditions is 4.9 A.m^{-2}. In this case, high strength molasses wastewater provided a particularly high COD concentration of 127,500 mg O_2.L^{-1} (He et al., 2017).

The maximum current density reached in the absence of N_2 bubbling was only 2.3 ± 0.5 A.m^{-2}. This lower performance was probably due to the aerobic consumption of COD in the reactors left open to air (no N_2 bubbling), which resulted in COD values of only 88 ± 15 mg O_2.L^{-1} at the end of the initial 28-day anodic phase, while average COD was 183 ± 32 mg O_2.L^{-1} in the reactors under N_2. The oxidation of the organic matter by oxygen explained why the concentration of dissolved oxygen was 0 mg/L, 10 cm under the free surface even in the absence of N_2 bubbling.

After day 28, successive anodic and cathodic phases were alternated (Fig. 1). The cathodic phases on days 28, 35, 38 and 44 (Fig. 2.B) lasted for around 24 h, during which time air was bubbled through all reactors. The anodic phases confirmed that the current density was 2 to 3 times higher in the reactors under N_2 than in those without N_2 bubbling. Anodes under N_2 reached a maximum of 5.5 ± 1.2 A.m^{-2}, which was at the highest level of current density obtained in real WW. The final values of anodic current density (day 52) exceeded those obtained during the period of biofilm formation before the anoxic/oxic alternations were started (day 28). This shows that the successive switches to cathodic conditions improved the anode performance. As already reported in the literature, operating in bidirectional mode with aerobic phases can enhance the performance of organic matter oxidation (Blanchet et al., 2014; Chen et al., 2019a; Freguia et al., 2008).

On day 40, nitrogen bubbling was stopped for 2 days. The current density produced by the reactors normally under N_2 dropped until it reached the values of the reactor without N_2, around 2.0 A.m^{-2}. Conversely, from day 49, all the reactors were placed under N_2. The reactors that had not benefited from N_2 until that time reached the same current density level as the reactors that had been operated under N_2, with current densities up to 4.0 A.m^{-2}. In this case, the average CODs were of the same order, 156 ± 11 mg O_2.L^{-1} and 164 ± 19 mg O_2.L^{-1}, respectively. These two symmetrical checks (no N_2 bubbling in any reactor on day 40 and N_2 bubbling in all reactors on day 49) showed that the presence or absence of N_2 supply during biofilm formation and the anodic phases did not significantly affect the biofilm electroactive capability since all electrodes produced similar current density when they were placed in the same conditions. The conditions of N_2 bubbling or no N_2 bubbling during the anodic phases affected the current produced mainly through the aerobic consumption of COD.

In the reactors with N_2, pH was stable even during phase changes,

with an average value of 8.6 ± 0.3 at the end of the anodic phases and 8.6 ± 0.1 during the cathodic phases. In reactors without N_2, the pH varied slightly, with 7.6 ± 0.1 and 8.3 ± 0.1 during the anodic and cathodic phases, respectively. The pH increase in the reactors without N_2 during the anodic phases may have been due to the production of CO_2 by oxidation of organic matter, which acidified the medium. During the cathodic phases, the air bubbling flushed CO_2 and the pH returned to its initial value. On the contrary, in the reactors under N_2, the continuous bubbling evacuated the CO_2 produced and maintained a stable value of pH.

During forced aeration, the concentration of dissolved oxygen was maintained at 6.8 ± 0.5 mg/L. When the aeration started, the current density dropped rapidly until it reached negative values corresponding to the cathode mode. The cathodic current density stabilised in the 0.05–0.10 A.m^{-2} range when there was no N_2 supply during the anode phases. Reactors under N_2 during the anode phases showed a weaker ability to switch to cathode mode. Cathodic current densities were lower, not exceeding 0.05 A.m^{-2}, while some reactors kept a slightly anodic behaviour. Cathodic currents were always considerably lower than the anodic currents. It has already been reported in the literature that cathodic currents are generally considerably lower than anodic currents, whether the electron acceptor is oxygen (Blanchet et al., 2014) or not (Yang et al., 2017).

At the end of the cathodic phases, when all the reactors were under air bubbling, the average COD measurements were similar for all the reactors, with 84 ± 17 mg O_2.L^{-1} and 86 ± 10 mg O_2.L^{-1} in the reactors operated with and without N_2, respectively. This fraction represents the refractory COD, which could not be degraded by bacteria, even after 24 h of intensive aeration.

Cyclic voltammetries recorded at day 48, during the fourth cathodic phase, are reported in Fig. 3. CVs displayed clear waves of oxygen reduction, with reduction current density greater than 1.5 A.m^{-2} at -0.3 V vs. SCE. The electrodes subjected to N_2 bubbling during the anodic phases showed a plateau around this value of current density (Fig. 3.A). In contrast, the electrodes formed without N_2 supply produced continuously increasing current density at lower potentials, with no plateau, up to -3.7 A.m^{-2}, at -0.6 V vs. SCE (Fig. 3.B). These kinetics were less than those reported for the very best mono-directional O_2-reducing microbial cathodes, which reached 2 to 2.5 A.m^{-2} (Wang et al., 2013; Izadi et al., 2019) when developed on gas-diffusion electrodes, and up to 3 A.m^{-2} at 0.4 V vs Ag/AgCl under forced aeration (Milner and Yu, 2018). Nevertheless, they can be reasonably compared with efficient conventional O_2-reducing microbial cathodes. The electrodes operated under N_2 and without N_2 were consequently able to reduce oxygen efficiently in cathodic conditions, but those formed under N_2 showed a limiting current at the lower potential values.

At day 49, when the anodic conditions were restored, CVs showed that the electrodes under N_2 rapidly displayed anodic behaviour, with currents up to around 11 A.m^{-2} at 0.4 V vs. SCE (Fig. 3.A). In contrast, the electrodes operating without N_2 were hard to return to anodic behaviour and their current densities did not reach 2 A.m^{-2} (Fig. 3.B). At day 49, all the reactors were placed under N_2 bubbling and CVs were recorded again at day 52. The electrodes usually operating under N_2 gave CVs that looked the same as those recorded on day 48, while the electrodes usually operating without N_2 showed considerably improved performance, with current densities reaching 7 A.m^{-2}. As mentioned above, the lower performance of the anodes operating without N_2 supply was mainly due to the side consumption of COD by aerobic bacteria. When put under N_2, these anodes clearly showed better performance, even if they did not quite reach those of the electrodes continuously operated under N_2.

To sum up the electrochemical part of this work, information that holds great promise must be kept in mind if the objective is to design ABMEs in the form of MFCs or microbial snorkels suitable for working in WW treatment tanks. It has been demonstrated here, for the first time, that raw WW have the capacity to form efficient ABMEs without the
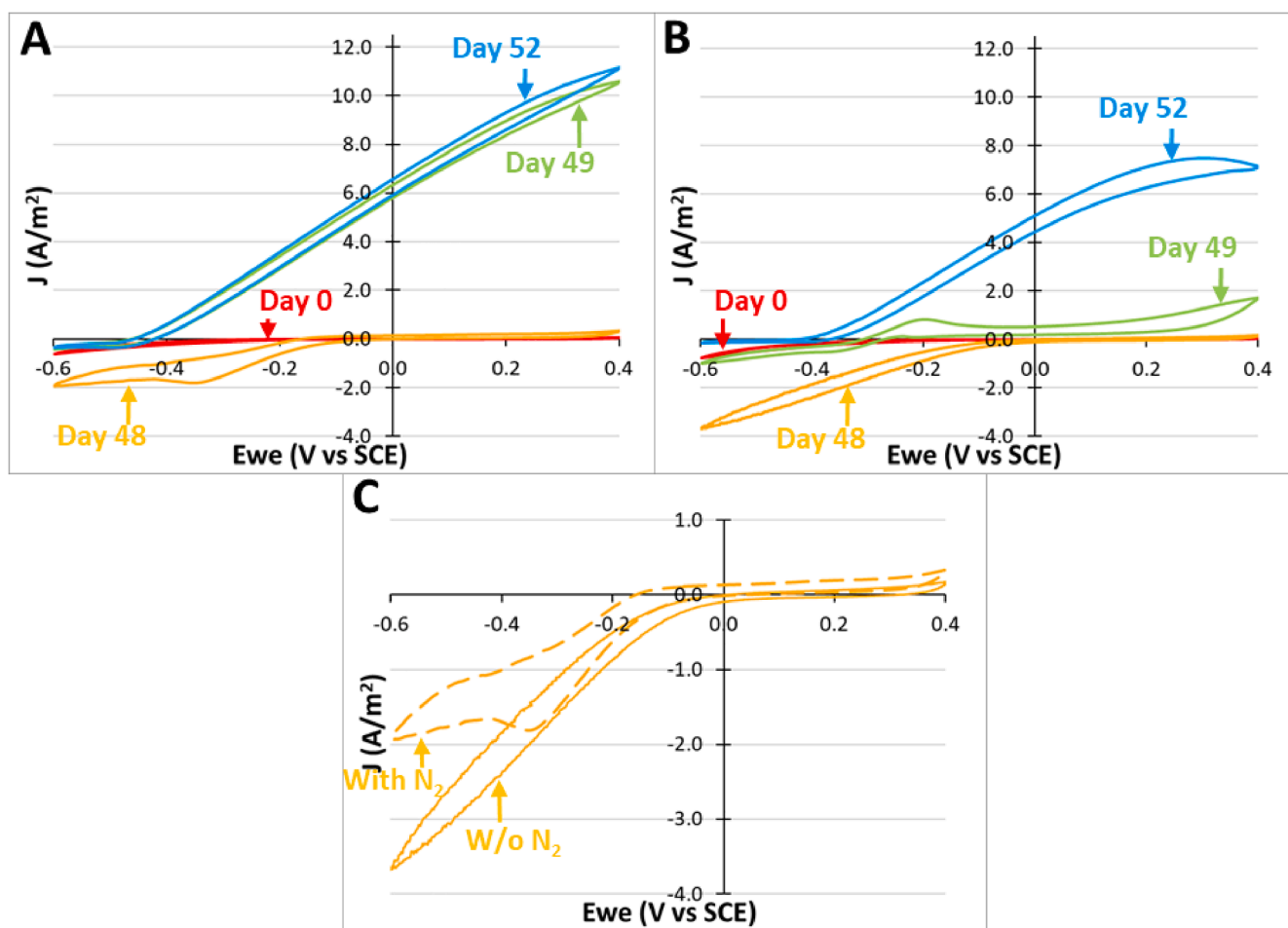
Fig. 3. Cyclic Voltammetries recorded at 1 mV/s on day 0 (initial), day 48 (cathodic phase, under aeration), day 49 (anodic phase) and day 52 (all reactors were under N_2 bubbling). (A) N_2 bubbling during the anodic phases; (B) no N_2 during the anodic phases; (C) Comparison of the CVs on day 48 extracted from A) and B).

addition of any substrate. The ABMEs produced anodic current density at a level matching the highest magnitudes reported in the literature for conventional microbial anodes formed in raw WW. The periodic shift to aerated conditions did not disturb their exoelectrogenic capacities, which were recovered when aeration was stopped. Notably, the catalysis of oxygen reduction was more efficient when the biofilms were not operated in strictly anaerobic conditions during the anode phases. Nitrogen bubbling was consequently not useful, and could even be detrimental, for designing ABMEs. This is important and encouraging information for the possible scale up of ABMEs to large sized installations.

3.2. Microbial population analysis

3.2.1. Diversity of microbial communities

Sequencing data were first examined at the class level. Archaea represented less than 0.5% of the DNA of the samples. Three major bacterial classes were present in all samples: *Gammaproteobacteria* from the *Proteobacteria* phylum, *Bacteroidia* from the *Bacteroidetes,* and *Clostridia* from the *Firmicutes* (Fig. 4). *Gammaproteobacteria* abundances were higher in the culture medium (up to 62%) than in the internal biofilm (up to 50%). Logically, the external biofilm, which is located at the interface between the internal biofilm and the culture medium, presented intermediate values. *Clostridia* showed the same behaviour as the *Gammaproteobacteria* regarding the biomass location, with values up to 21% in the culture medium, dropping to 14% maximum in the external biofilm and less that 10% in the internal one. The *Bacteroidia* class showed opposite results with higher abundance (up to 57%) in the

internal biofilm than in the culture medium (40% maximum at day 52).

Relative abundance of the different classes was influenced by N_2 supply. In the reactors under N_2, the *Gammaproteobacteria* class was the most abundant, with up to 62%, whereas the *Bacteroidia* class was the most abundant in the reactors without N_2 bubbling (50% maximum). The abundances of *Clostridia* tended to be higher for the reactors without N_2 but the effect of N_2 seemed less marked than that found for the *Gammaproteobacteria*. *Gammaproteobacteria* have already been described in bioelectrochemical systems (BESs) including both exoelectrogenic and electrotrophic species (Logan et al., 2019). These differences in the microbial populations may support the lower O_2 reduction capability that was observed with the electrodes formed under N_2 during the anode phases. Fig. 5 represents the most abundant genera in the *Gammaproteobacteria* class. The major genus found here is *Acinetobacter*, an electrotrophic species. It grows preferentially in the culture medium rather than in biofilm and is more abundant in the reactors with N_2, except for the internal biofilm at day 52.

A total of 49 OTUs from the *Acinetobacter* genus were found here, confirming the large presence of this genus. The major one, OTU_1 had an abundance of up to 35% in the samples from the culture medium, but could not be affiliated up to the species level. Different species of this aerobic genus have already been identified in wastewater treatment plants (Liu et al., 2017; Chen et al., 2019b), including BESs (Sathishkumar et al., 2019). The *Acinetobacter* genus has already been identified in O_2-reducing bidirectional biofilms (Blanchet et al., 2014; Yun et al., 2018) with, in these cases too, a higher abundance in the culture medium.

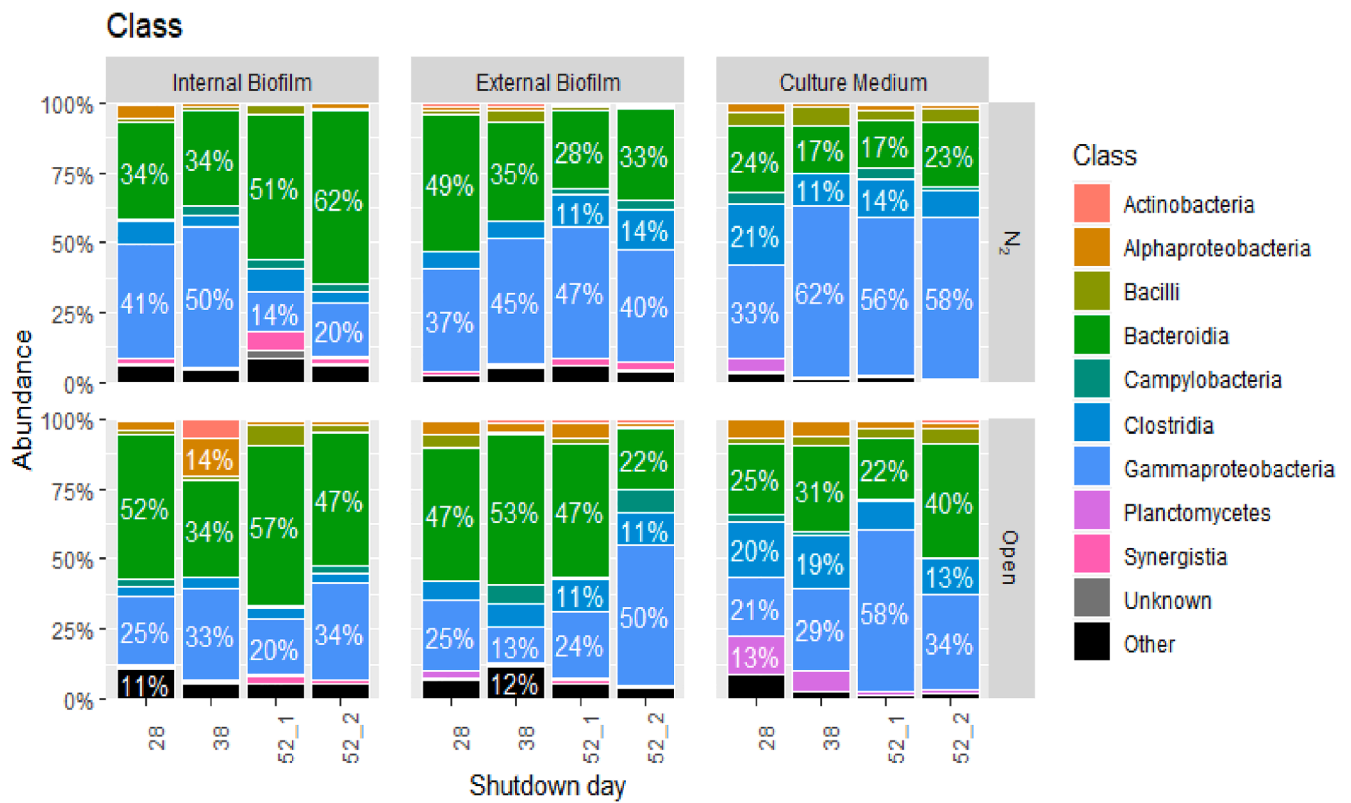The main bacterial genus usually found in most microbial

Fig. 4. Relative abundances of the classes. Top line: reactors under N$_2$ bubbling; bottom line: reactors without N$_2$ supply, open to air. For each condition, samples were collected at day 28 (end of the anode formation phase), day 38 before the third cathodic phase, and day 52 at the end of the experiment (52_1 and 52_2 are duplicates).
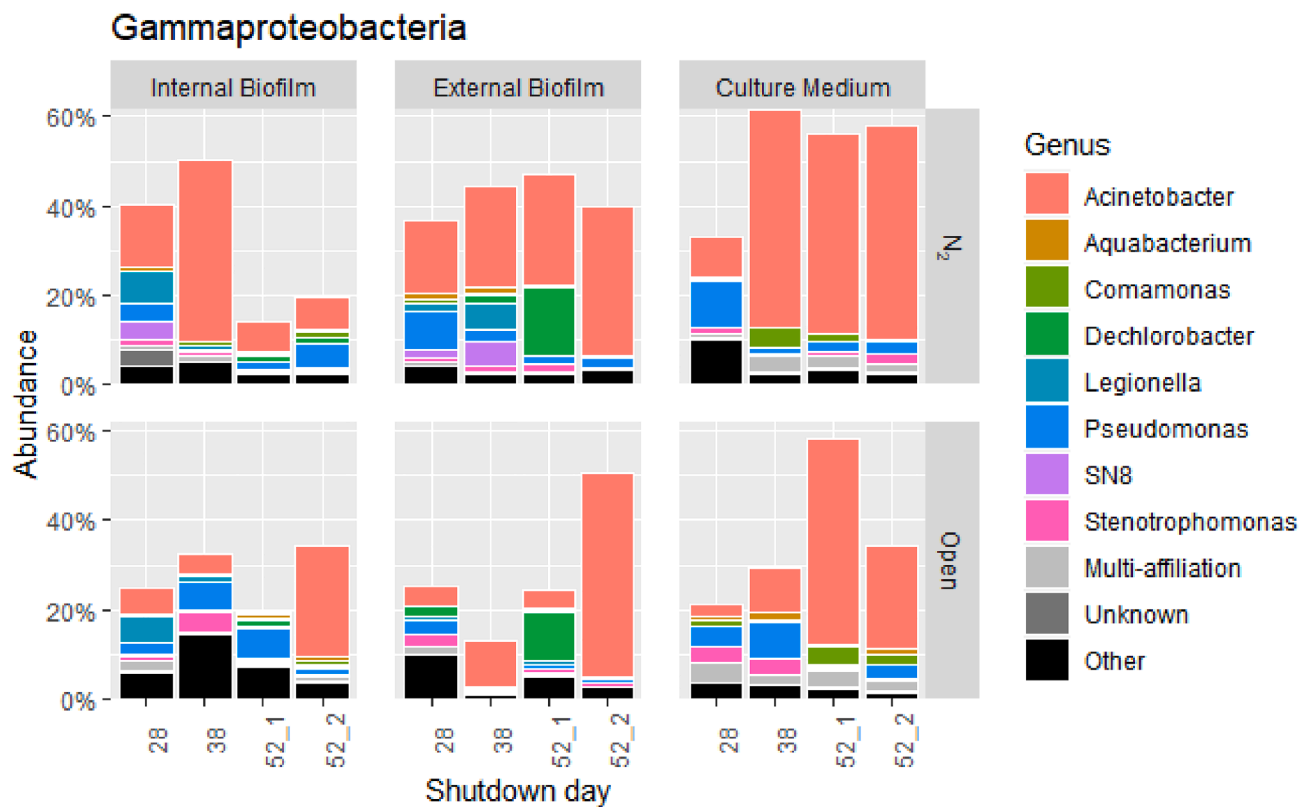

Fig. 5. Principal genera in the *Gammaproteobacteria* class.

electrochemical systems, *Geobacter* (Logan et al., 2019; Roubaud et al., 2019; Yun et al., 2018), was absent here. As *Geobacter* species are anaerobic, intense aeration during the cathodic phases was most probably detrimental to the development of the genus. Here, other electroactive bacteria, such as *Acinetobacter* or *Pseudomonas*, aerobic or facultative anaerobic, should ensure the electron transfers.

For the *Bacteroidia* and *Clostridia* classes, the diversity of the genera was greater and Principal Component Analysis (PCA) was carried out to refine the analysis at the OTU level.

3.2.2. Comparison of the samples based on the aeration, biomass location and biofilm age

PCA was carried out on the 16SRNA gene tag datasets. Plots of individuals, representing each sample (Fig. 6.A and 6.C), show the separation of the different samples according to the PCA (components 1, 2 and 3). Samples from the culture medium are clearly distinguished from the biofilm samples (component 1). The difference is less clear between internal and external biofilm samples, indicating that the biofilms over and inside the electrode have close microbial populations. Samples collected at the end of the biofilm formation phase (day 28) were separated from the samples taken later on (component 2). This shows that the anoxic/oxic alternations, which started after day 28, affected the microbial populations.

Component 3 separated samples according to the N_2 bubbling and independently of their type, except for the internal biofilm at day 52. The internal biofilm at day 52 could act differently because it was not exposed to the influence of aeration in the same way as the other samples, especially after 52 days of experiment.

The correlation circles were used to link the observed patterns to the microbial dynamics and evolution of bacterial abundances between the
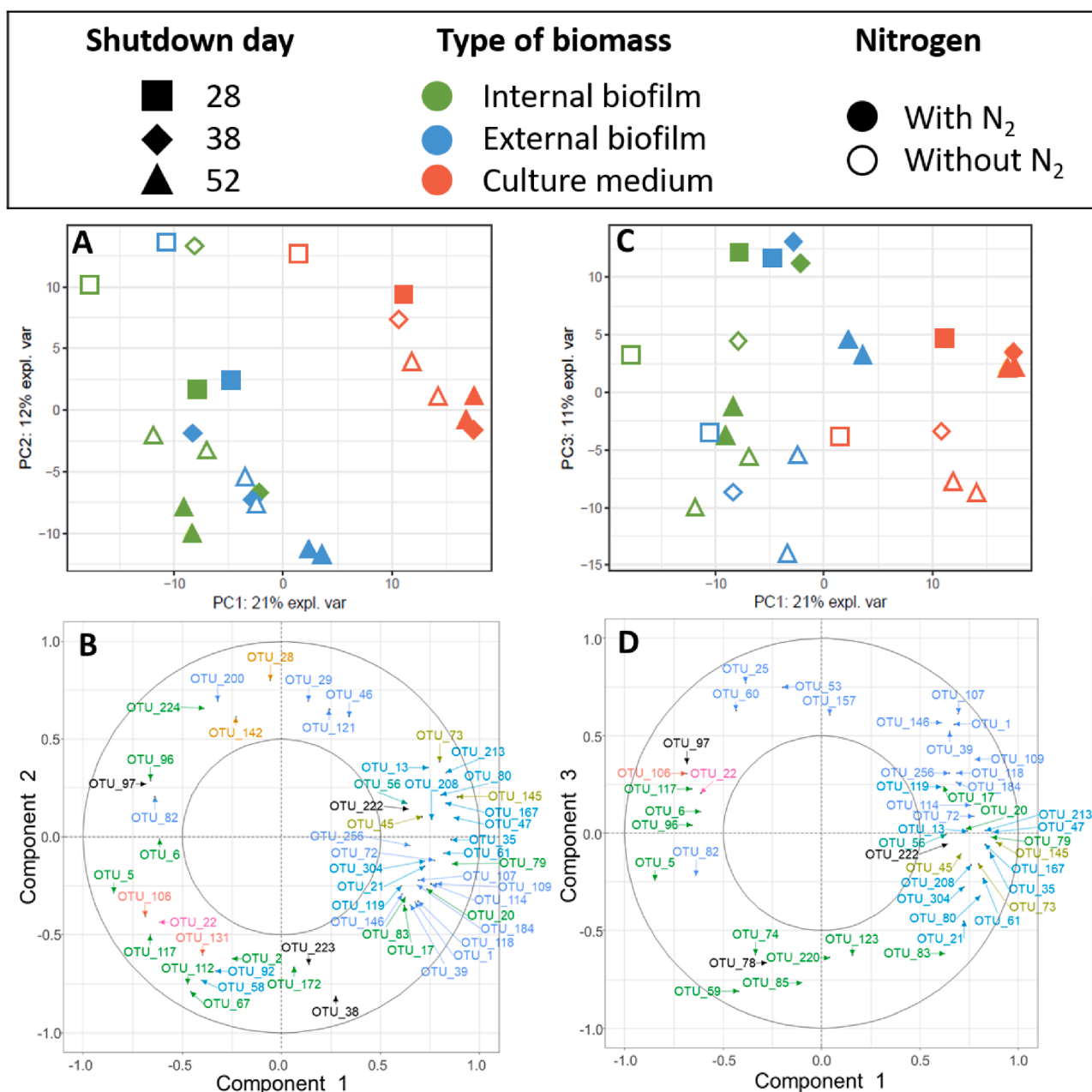

Fig. 6. Comparison of samples based on the biofilm location and age, plot of individuals (A) and correlation circle (B); based on the biofilm location and N_2 bubbling, plot of individuals (C) and correlation circle (D). NB: OTUs on the correlation circles (B and D) are coloured according to the bacterial class, with the same colours as those used in Fig. 3.

samples (Fig. 6B and D). According to component 1, a large bacterial diversity was characteristic of the media, with a majority of OTUs from the *Gammaproteobacteria* and *Clostridia* classes. Among them, OTU_35 *Proteiniclasticum* genus, *Clostridia* class, is a hydrogen autotrophic bacterium, known to degrade protein in BESs using wastewater (Yin et al., 2017; Gao et al., 2020). It could replace *Geobacter* in the present system. *Pseudomonas* (OTU_256, *Gamma-proteobacteria*), also characteristic of the media, is known for its heterotrophic nitrification and aerobic denitrification capabilities (Chen et al., 2019b) and its speculated ability to catalyse the electrochemical oxygen reduction (Blanchet et al., 2014).

Some OTUs from the *Bacteroidia* class *Cloacibacterium* were characteristic of the biofilm samples. Among them, OTU_6 is a facultative anaerobe that can adapt to the alternation phase without suffering from a lack or an excess of O_2. It was originally found in wastewater and is known to be electroactive, contributing to organic compound degradation in BESs using activated sludge as the inoculum (Gao et al., 2020; Zheng et al., 2019) or a consortium from phenol polluted wastewater (Hassan et al., 2018).

On component 2, *Brevundimonas* (OTU_28, *Bacilli*), characteristic of the samples at day 28, is from the *Caulobacteraceae* family, observed in BESs used for advanced oxidation in water treatment (Bennani et al., 2015). *Paludibacter* (OTU_172, *Bacteroidia*), characteristic of more advanced dates, has been found as part of the biocathode community in a bidirectional electrode operated in domestic wastewater (Yun et al., 2018). This could explain why it is characteristic of late sampling dates, after several anodic–cathodic alternations. It might also play a role in sulfate removal in BESs (Liang et al., 2013).

According to component 3, a characteristic OTU of the reactors without N_2 bubbling is *Pseudomonas* (OTU_157, *Gammaproteobacteria*), as described earlier. The *Lentimicrobiaceae* family (OTU_220, *Bacteroidia*), characteristic of the reactors without N_2, has already been observed in a BES implemented for COD removal (De Paepe et al., 2020).

In summary, the most influential parameter in the present system is the biofilm/medium location, with a clear separation between the culture medium and the biofilm (both internal and external). Date of sampling is the second parameter responsible for an important difference between samples from biofilm formation phase (day 28) and alternation phase (days 38 and 52). Finally, a difference between the samples from the reactors with and without N_2 was observed. The very large variety of taxa present in the samples, both in terms of abundance and variance, was probably the cause of the stability and high values of both cathodic and anodic currents. The present and characteristic OTUs were a mixture of anaerobic species, often found in anaerobic digesters, and aerobic species, found in biocathodes. All of them have already been identified separately in BESs.

To the best of our knowledge, only one previous study has analysed the microbial population of a bidirectional electrode designed in wastewater (Chen et al., 2019a). A different biofilm structure was reported, with aerobes in the external layer (including genus *Neomegalonema, Alphaproteobacteria* class) and exoelectrogens in the internal one (including genus *Arcobacter* of the *Epsilonproteobacteria* class) whereas, in our study, no significant difference was found between the internal and external biofilms and the microorganisms described previously in ABMEs were not identified here. These differences may stem from the different experimental set-ups and protocols. This shows that different ways can result in efficient mixes of aerobic and anaerobic species, working together in bidirectional biofilms designed in real wastewater.

All the experiments were performed under constant, controlled potential here. This means that the effects observed (summarized in the conclusion below) were the direct consequences of the anoxic/oxic conditions and were not indirectly induced by the variations of the potential value that can be provoked by the different anoxic/oxic conditions. Actually, the potential of the electrodes can vary in different ways and to different extents depending on the type (MFC, snorkel, electrolysis cell) and the design (ratio of anode/cathode surface areas, distance

between anode and cathode, external resistance in MFC…) of the set-ups. Now, similar experiments can be carried out with different cell types and compared to the basis described here in order to unravel the indirect effects of the variations of the potential, which are linked to the cell configuration, and the direct effects of the anoxic/oxic conditions, which have been characterised here.

4. Conclusion

Raw domestic wastewater showed the capacity to form efficient ABMEs. Putting the reactor under N_2 during the anodic phases revealed higher anodic currents, because it avoided the side-consumption of COD by aerobic bacteria, but it did not improve the intrinsic anodic capacity of the ABMEs and it was detrimental to the cathodic currents. Strictly anaerobic conditions are consequently not required for the design of ABMEs. The electrode efficiency and stability was explained by the large variety of the microbial population, which mixed – in the same biofilm –aerobic and anaerobic species that have already been identified separately in different bioelectrochemical microbiotas.

CRediT authorship contribution statement

Morgane Hoareau: Investigation, Writing - original draft, Writing - review & editing, Visualization. **Benjamin Erable:** Conceptualization, Methodology, Validation, Writing - review & editing, Supervision. **Olivier Chapleur:** Formal analysis, Visualization, Writing - review & editing, Supervision. **Cédric Midoux:** Formal analysis, Visualization, Writing - review & editing. **Chrystelle Bureau:** Investigation, Writing - review & editing. **Anne Goubet:** Investigation, Writing - review & editing. **Alain Bergel:** Conceptualization, Methodology, Validation, Writing - original draft, Writing - review & editing, Visualization, Supervision, Funding acquisition.

Declaration of Competing Interest

The authors declare that they have no known competing financial interests or personal relationships that could have appeared to influence the work reported in this paper.

Appendix A. Supplementary data

Supplementary data to this article can be found online at https://doi.org/10.1016/j.biortech.2021.124663.

References

Aguirre-Sierra, A., Bacchetti-De Gregoris, T., Berná, A., Salas, J.J., Aragón, C., Esteve-Núñez, A., 2016. Microbial electrochemical systems outperform fixed-bed biofilters in cleaning up urban wastewater. Environ. Sci. Water Res. Technol. 2 (6), 984–993. https://doi.org/10.1039/C6EW00172F.

Bennani, Y., Peters, M.C.F.M., Appel, P.W., Rietveld, L.C., 2015. Electrochemically active biofilm and photoelectrocatalytic regeneration of the titanium dioxide composite electrode for advanced oxidation in water treatment. Electrochim. Acta 182, 604–612. https://doi.org/10.1016/j.electacta.2015.09.101.

Blanchet, E., Erable, B., De Solan, M.-L., Bergel, A., 2016. Two-dimensional carbon cloth and three-dimensional carbon felt perform similarly to form bioanode fed with food waste. Electrochem. Commun. 66, 38–41. https://doi.org/10.1016/j.elecom.2016.02.017.

Blanchet, E., Pécastaings, S., Erable, B., Roques, C., Bergel, A., 2014. Protons accumulation during anodic phase turned to advantage for oxygen reduction during

cathodic phase in reversible bioelectrodes. Bioresour. Technol. 173, 224–230. https://doi.org/10.1016/j.biortech.2014.09.076.

Chen, S., Brown, R.K., Patil, S.A., Huber, K.J., Overmann, J., Schröder, U., 2019a. Aerobic microbial electrochemical technology based on the coexistence and interactions of aerobes and exoelectrogens for synergistic pollutant removal from wastewater. Environ. Sci. Water Res. Technol. 5 (1), 60–69. https://doi.org/10.1039/C8EW00530C.

Chen, S., He, S., Wu, C., Du, D., 2019b. Characteristics of heterotrophic nitrification and aerobic denitrification bacterium Acinetobacter sp. T1 and its application for pig farm wastewater treatment. J. Biosci. Bioeng. 127 (2), 201–205. https://doi.org/10.1016/j.jbiosc.2018.07.025.

Cheng, K.Y., Ho, G., Cord-Ruwisch, R., 2010. Anodophilic biofilm catalyzes cathodic oxygen reduction. Environ. Sci. Technol. 44 (1), 518–525. https://doi.org/10.1021/es9023833.

De Paepe, J., De Paepe, K., Gòdia, F., Rabaey, K., Vlaeminck, S.E., Clauwaert, P., 2020. Bio-electrochemical COD removal for energy-efficient, maximum and robust nitrogen recovery from urine through membrane aerated nitrification. Water Res. 185, 116223. https://doi.org/10.1016/j.watres.2020.116223.

Domínguez-Garay, A., Esteve-Núñez, A., 2018. Designing strategies for operating microbial electrochemical systems to clean up polluted soils under non-flooded conditions. Bioelectrochemistry 124, 142–148. https://doi.org/10.1016/j.bioelechem.2018.03.006.

Erable, B., Bergel, A., 2009. First air-tolerant effective stainless steel microbial anode obtained from a natural marine biofilm. Bioresour. Technol. 100 (13), 3302–3307. https://doi.org/10.1016/j.biortech.2009.02.025.

Erable, B., Etcheverry, L., Bergel, A., 2011. From microbial fuel cell (MFC) to microbial electrochemical snorkel (MES): maximizing chemical oxygen demand (COD) removal from wastewater. Biofouling 27 (3), 319–326. https://doi.org/10.1080/08927014.2011.564615.

Escudié, F., Auer, L., Bernard, M., Mariadassou, M., Cauquil, L., Vidal, K., Maman, S., Hernandez-Raquet, G., Combes, S., Pascal, G., 2018. FROGS: find, rapidly, OTUs with galaxy solution. Bioinformatics 34, 1287–1294. https://doi.org/10.1093/bioinformatics/btx791.

Freguia, S., Rabaey, K., Yuan, Z., Keller, J., 2008. Sequential anode–cathode configuration improves cathodic oxygen reduction and effluent quality of microbial fuel cells. Water Res. 42 (6-7), 1387–1396. https://doi.org/10.1016/j.watres.2007.10.007.

Gao, Y., Huang, H., Peng, C., Fan, X., Hu, J., Ren, H., 2020. Simultaneous nitrogen removal and toxicity reduction of synthetic municipal wastewater by micro-electrolysis and sulfur-based denitrification biofilter. Bioresour. Technol. 316, 123924. https://doi.org/10.1016/j.biortech.2020.123924.

Hassan, H., Jin, B.o., Donner, E., Vasileiadis, S., Saint, C., Dai, S., 2018. Microbial community and bioelectrochemical activities in MFC for degrading phenol and producing electricity: microbial consortia could make differences. Chem. Eng. J. 332, 647–657. https://doi.org/10.1016/j.cej.2017.09.114.

He, L.i., Du, P., Chen, Y., Lu, H., Cheng, X.i., Chang, B., Wang, Z., 2017. Advances in microbial fuel cells for wastewater treatment. Renew. Sustain. Energy Rev. 71, 388–403. https://doi.org/10.1016/j.rser.2016.12.069.

Hoareau, M., Erable, B., Bergel, A., 2019. Microbial electrochemical snorkels (MESs): a budding technology for multiple applications. A mini review. Electrochem. Commun. 104, 106473. https://doi.org/10.1016/j.elecom.2019.05.022.

Izadi, P., Fontmorin, J.-M., Fernández, L.F.L., Cheng, S., Head, I., Yu, E.H., 2019. High performing gas diffusion biocathode for microbial fuel cells using acidophilic iron oxidizing bacteria. Front. Energy Res. 7 https://doi.org/10.3389/fenrg.2019.00093.

Jiang, Y., Zeng, R.J., 2019. Bidirectional extracellular electron transfers of electrode-biofilm: Mechanism and application. Bioresour. Technol. 271, 439–448. https://doi.org/10.1016/j.biortech.2018.09.133.

Kalathil, S., Pant, D., 2016. Nanotechnology to rescue bacterial bidirectional extracellular electron transfer in bioelectrochemical systems. RSC Adv. 6 (36), 30582–30597. https://doi.org/10.1039/C6RA04734C.

Li, W., Sun, J., Hu, Y., Zhang, Y., Deng, F., Chen, J., 2014. Simultaneous pH self-neutralization and bioelectricity generation in a dual bioelectrode microbial fuel cell under periodic reversion of polarity. J. Power Sources 268, 287–293. https://doi.org/10.1016/j.jpowsour.2014.06.047.

Liang, F., Xiao, Y., Zhao, F., 2013. Effect of pH on sulfate removal from wastewater using a bioelectrochemical system. Chem. Eng. J. 218, 147–153. https://doi.org/10.1016/j.cej.2012.12.021.

Liu, H., Lu, Q., Wang, Q., Liu, W., Wei, Q., Ren, H., Ming, C., Min, M., Chen, P., Ruan, R., 2017. Isolation of a bacterial strain, Acinetobacter sp. from centrate wastewater and study of its cooperation with algae in nutrients removal. Bioresour. Technol. 235, 59–69. https://doi.org/10.1016/j.biortech.2017.03.111.

Logan, B.E., Rossi, R., Ragab, A., Saikaly, P.E., 2019. Electroactive microorganisms in bioelectrochemical systems. Nat. Rev. Microbiol. 17 (5), 307–319. https://doi.org/10.1038/s41579-019-0173-x.

Madigou, C., Lê Cao, K.-A., Bureau, C., Mazéas, L., Déjean, S., Chapleur, O., 2019. Ecological consequences of abrupt temperature changes in anaerobic digesters. Chem. Eng. J. 361, 266–277. https://doi.org/10.1016/j.cej.2018.12.003.

MIGALE, 2020. Migale Bioinformatics Facility. https://doi.org/10.15454/1.5572390655343293E12.

Milner, E.M., Popescu, D., Curtis, T., Head, I.M., Scott, K., Yu, E.H., 2016. Microbial fuel cells with highly active aerobic biocathodes. J. Power Sources 324, 8–16. https://doi.org/10.1016/j.jpowsour.2016.05.055.

Milner, E.M., Yu, E.H., 2018. The effect of oxygen mass transfer on aerobic biocathode performance, biofilm growth and distribution in microbial fuel cells. Fuel Cells 18 (1), 4–12. https://doi.org/10.1002/fuce:201700172.

Oliot, M., Galier, S., Roux de Balmann, H., Bergel, A., 2016. Ion transport in microbial fuel cells: key roles, theory and critical review. Appl. Energy 183, 1682–1704. https://doi.org/10.1016/j.apenergy.2016.09.043.

Poirier, S., Desmond-Le Quéméner, E., Madigou, C., Bouchez, T., Chapleur, O., 2016. Anaerobic digestion of biowaste under extreme ammonia concentration: identification of key microbial phylotypes. Bioresour. Technol. 207, 92–101. https://doi.org/10.1016/j.biortech.2016.01.124.

Rodrigo Quejigo, J., Tejedor-Sanz, S., Esteve-Núñez, A., Harnisch, F., 2019. Bed electrodes in microbial electrochemistry: setup, operation and characterization. ChemTexts 5 (1). https://doi.org/10.1007/s40828-019-0078-3.

Rimboud, M., Pocaznoi, D., Erable, B., Bergel, A., 2014. Electroanalysis of microbial anodes for bioelectrochemical systems: basics, progress and perspectives. PCCP 16 (31), 16349–16366. https://doi.org/10.1039/C4CP01698J.

Rohart, F., Gautier, B., Singh, A., Lê Cao, K.-A., 2017. mixOmics: An R package for 'omics feature selection and multiple data integration. PLOS Comput. Biol. 13, e1005752. https://doi.org/10.1371/journal.pcbi.1005752.

Roubaud, E., Lacroix, R., Da Silva, S., Etcheverry, L., Bergel, A., Basséguy, R., Erable, B., 2019. Benchmarking of industrial synthetic graphite grades, carbon felt, and carbon cloth as cost-efficient bioanode materials for domestic wastewater fed microbial electrolysis cells. Front. Energy Res. 7 https://doi.org/10.3389/fenrg.2019.00106.

Sathishkumar, K., AlSalhi, M.S., Sanganyado, E., Devanesan, S., Arulprakash, A., Rajasekar, A., 2019. Sequential electrochemical oxidation and bio-treatment of the azo dye congo red and textile effluent. J. Photochem. Photobiol., B 200, 111655. https://doi.org/10.1016/j.jphotobiol.2019.111655.

Strik, D.P.B.T.B., Hamelers, H.V.M., Buisman, C.J.N., 2010. Solar energy powered microbial fuel cell with a reversible bioelectrode. Environ. Sci. Technol. 44 (1), 532–537. https://doi.org/10.1021/es902435v.

Sun, J., Hu, Y., Li, W., Zhang, Y., Chen, J., Deng, F., 2015. Sequential decolorization of azo dye and mineralization of decolorization liquid coupled with bioelectricity generation using a pH self-neutralized photobioelectrochemical system operated with polarity reversion. J. Hazard. Mater. 289, 108–117. https://doi.org/10.1016/j.jhazmat.2015.02.010.

Wang, Z., Zheng, Y., Xiao, Y., Wu, S., Wu, Y., Yang, Z., Zhao, F., 2013. Analysis of oxygen reduction and microbial community of air-diffusion biocathode in microbial fuel cells. Bioresour. Technol. 144, 74–79. https://doi.org/10.1016/j.biortech.2013.06.093.

Xie, Q., Lu, Y., Tang, L., Zeng, G., Yang, Z., Fan, C., Wang, J., Atashgahi, S., 2020. The mechanism and application of bidirectional extracellular electron transport in the field of energy and environment. Crit. Rev. Env. Sci. Technol. 1–46. https://doi.org/10.1080/10643389.2020.1773728.

Yang, G., Huang, L., You, L., Zhuang, L.i., Zhou, S., 2017. Electrochemical and spectroscopic insights into the mechanisms of bidirectional microbe-electrode electron transfer in Geobacter soli biofilms. Electrochem. Commun. 77, 93–97. https://doi.org/10.1016/j.elecom.2017.03.004.

Yang, L.-H., Zhu, T.-T., Cai, W.-W., Haider, M.R., Wang, H.-C., Cheng, H.-Y., Wang, A.-J., 2018. Micro-oxygen bioanode: An efficient strategy for enhancement of phenol degradation and current generation in mix-cultured MFCs. Bioresour. Technol. 268, 176–182. https://doi.org/10.1016/j.biortech.2018.07.025.

Yin, Q., Miao, J., Li, B.o., Wu, G., 2017. Enhancing electron transfer by ferroferric oxide during the anaerobic treatment of synthetic wastewater with mixed organic carbon. Int. Biodeterior. Biodegrad. 119, 104–110. https://doi.org/10.1016/j.ibiod.2016.09.023.

Yong, X.-Y., Yan, Z.-Y., Shen, H.-B., Zhou, J., Wu, X.-Y., Zhang, L.-J., Zheng, T., Jiang, M., Wei, P., Jia, H.-H., Yong, Y.-C., 2017. An integrated aerobic-anaerobic strategy for performance enhancement of Pseudomonas aeruginosa-inoculated microbial fuel cell. Bioresour. Technol. 241, 1191–1196. https://doi.org/10.1016/j.biortech.2017.06.050.

Yu, Y., Wu, Y., Cao, B., Gao, Y.-G., Yan, X., 2015. Adjustable bidirectional extracellular electron transfer between Comamonas testosteroni biofilms and electrode via distinct electron mediators. Electrochem. Commun. 59, 43–47. https://doi.org/10.1016/j.elecom.2015.07.007.

Yun, H., Liang, B., Kong, D., Wang, A., 2018. Improving biocathode community multifunctionality by polarity inversion for simultaneous bioelectroreduction processes in domestic wastewater. Chemosphere 194, 553–561. https://doi.org/10.1016/j.chemosphere.2017.12.030.

Zheng, M., Xu, C., Zhong, D., Han, Y., Zhang, Z., Zhu, H., Han, H., 2019. Synergistic degradation on aromatic cyclic organics of coal pyrolysis wastewater by lignite activated coke-active sludge process. Chem. Eng. J. 364, 410–419. https://doi.org/10.1016/j.cej.2019.01.121.